METHODS:
Custom-developed Purkinje apparatus for phakometry and lens tilt and decentration

2

2. *Phakometry and lens tilt and decentration using a custom-developed Purkinje imaging apparatus: validation and measurements*

This chapter is based on the article by Rosales et al., *"Phakometry and lens tilt and decentration using a custom-developed Purkinje imaging apparatus: validation and measurements"* Journal of the Optical Society of America A. 2006. 23: p.509-520. Coauthor of the study is Susana Marcos. The contribution of Patricia Rosales to the study was to develop the Purkinje imaging system, to carry out the experiments to validate the system and the measurements of phakometry, tilt and decentration on patients, data analysis and the discussion of the results.

RESUMEN

Objetivos: Desarrollo de un sistema de detección de imágenes de Purkinje para la medida de radios de curvatura, inclinación y descentramiento del cristalino y lentes intraoculares. Se presenta una validación de la técnica a través de simulaciones computacionales, experimentos control y primeras medidas en 17 ojos normales (edad media: 26.67 ± 2.31 años) y nueve ojos de pacientes operados de cirugía de cataratas (edad media: 74 ± 2.3 años).

Métodos: Se ha diseñado un sistema de detección de imágenes de Purkinje que consiste en dos canales de iluminación, uno para el ojo derecho y otro para el izquierdo (con luz procedente de un único LED infrarrojo), con estos canales se mide la inclinación y el descentramiento, y otro canal de iluminación que consiste en dos LEDs infrarojos, para las medidas de facometría. Estas imágenes se capturan con una cámara sensible al infrarrojo con un objetivo telecéntrico para capturar las dobles imágenes de Purkinje reflejadas por las diferentes superficies oculares con los mismos aumentos. El sistema cuenta con un sistema de fijación que consiste en un "minidisplay" con resolución SVGA y un sistema de badal para la corrección de errores refractivos. Los radios de curvatura se obtuvieron a partir de estas imágenes empleando el Teorema del Espejo Equivalente y una función de Mérito. Para la obtención de la inclinación y el descentramiento se emplearon las ecuaciones de Phillips que consideran una relación lineal entre la posición de las imágenes de Purkinje, la rotación del ojo, el tilt y el descentramiento de la lente.

Resultados: Los valores de los radios de curvatura (±SD) medidos se encuentran entre 12.7±0.37 y 8.81± 0.21 mm y entre -5.64 ± 0.44 y -7.09±0.41 mm para las caras anterior y posterior del cristalino respectivamente. Los valores de inclinación del cristalino (±SD) se encuentran entre 2.8±0.4 y -2.87±0.34 deg en dirección horizontal y entre 2.58±0.27 y -1±0.31 deg en dirección vertical. Los valores de descentramiento (±SD) del cristalino obtenidos se encuentran entre 0.09±0.03 y 0.45±0.02 mm en dirección horizontal y entre 0.39±0.03 y

-0.22±0.82 mm en dirección vertical. La inclinación de las lentes intraoculares se encuentra entre 3.6±0.03 y -1.51±1.34 deg en dirección horizontal y entre 5.97±0.82 y -1.85±0.52 deg en la dirección vertical. El descentramiento de las lentes intraoculares se encuentra entre 0.53±0.06 y -0.31±0.23 mm en dirección horizontal y entre 0.13±0.08 y -0.96±0.07 mm en dirección vertical. Las medidas obtenidas para los radios de curvatura en promedio son de 10.61±1.13 y -6.15±0.41 mm, para las caras anterior y posterior del cristalino respectivamente, y de 11.21±0.86 y -11.3±0.91 para las caras anterior y posterior de la lente intraocular.

Conclusiones: Se ha desarrollado y validado mediante simulaciones computacionales un sistema para la detección de imágenes de Purkinje para la medida de radios de curvatura, inclinación y descentramiento en ojos de sujetos jóvenes con cristalino normal, y en pacientes operados de cirugía de cataratas. Tanto las validaciones como las medidas, muestran que las medidas obtenidas mediante este sistema son precisas, siendo el principal factor limitante, la asfericidad de las superficies oculares que producen una cierta sobre estimación del radio de curvatura. Las simulaciones muestran que las estimaciones tienen una precisión de 0.85 y 0.66 mm para el radio de la cara anterior de la lente y de 1.35 y 0.75 mm para el de la cara posterior, empleando tanto el método del espejo equivalente y la función de mérito respectivamente. La reproducibilidad de las medidas del radio de curvatura del cristalino es de 0.34 y 0.28 mm para las caras anterior y posterior del cristalino. Para la inclinación, la reproducibilidad es de 0.29 y 0.33 deg para la dirección horizontal y vertical respectivamente. Para el descentramiento, la reproducibilidad es de 0.03 y 0.02 mm para la dirección horizontal y vertical respectivamente. La reproducibilidad de las medidas de radios de curvatura de las lentes intraoculares es de 0.31 y 0.61 mm para las caras anterior y posterior de la lente introcular. Para la inclinación de lentes intraoculares la reproducibilidad es de 0.33 y 0.29 deg para la dirección horizontal y vertical respectivamente, y de 0.06 y 0.05 mm para el descentramiento en dirección horizontal y vertical respectivamente.

ABSTRACT

Purpose: We present a Purkinje Imaging system for phakometry and measurement of tilt and decentration of crystalline and intraocular lenses. We present a complete validation of the technique through exhaustive computer simulations and control experiments, and measurements in 17 normal eyes (mean age 26.67 ± 2.31 years) and 9 post-cataract surgery eyes (mean age 74±2.3 years).

Methods: The Purkinje imaging system consists of two illumination channels to illuminate the right and the left eye (with a single infrared LED each), to measure tilt and decentration, and other illuminating channel (with a double infrared LED) for phakometry measurements. Images of the eye with reflection of the LED's light from the different ocular surfaces (Purkinje images), were captured on a videocamera with an infrared sensitive CCD, and a telecentric lens to capture Purkinje images with the same magnification. The system also includes a fixation channel with a minidisplay and a Badal system to correct refractive errors. Lens radii of curvature were calculated using the equivalent mirror theorem and a merit function. To obtain lens tilt and decentration Phillips' equations were used, assuming a linear relation between the Purkinje images positions, rotation of the eye and lens tilt and decentration.

Results: Crystalline lens radii (±SD) ranged from 12.7±0.37 to 8.81± 0.21 mm and from -5.64 ± 0.44 to -7.09± 0.41 mm for anterior and posterior surface respectively. Crystalline lens tilt (±SD) ranged from 2.8±0.4 to -2.87±0.34 deg horizontally and 2.58±0.27 to -1±0.31 deg vertically. Crystalline lens decentration (±SD) ranged from 0.09±0.031 to 0.45±0.02 mm horizontally and from -0.22±0.82 mm to 0.39±0.03 mm vertically. IOL tilt ranged (±SD) from 3.6±0.03 to -1.51±1.34 deg horizontally and 5.97±0.08 to -1.85±0.52 deg vertically. IOL decentration (±SD) ranged from 0.53±0.06 to -0.31±0.23 mm horizontally and from 0.13±0.08 to -0.96±0.07 mm vertically.

Conclusions: A Purkinje imaging system has been developed and computationally validated for phakometry, lens tilt and decentration measurements, in phakic and pseudophakic eyes. Simulations and computational validations show that measurements obtained with this method are accurate. The asphericity of the ocular surfaces cause a certain overestimation of the lens radius of curvature, that can be avoided if Purkinje images are obtained near the pupil center where the ocular surfaces can be considered as spherical. Computer simulations show estimates should be accurate within 0.85 and 0.66 mm for the retrieved anterior lens radius of curvature, and within 1.35 and 0.75 mm for the retrieved posterior lens radius of curvature with the equivalent mirror and merit function methods, respectively, and within 0.25 deg and 0.013 mm for the retrieved lens tilt and decentration. Average reproducibility of lens radius of curvature measurement is 0.34 mm and 0.28 mm for the anterior and posterior surfaces of the phakic eye and 0.31 mm and 0.61 mm for the anterior and posterior surfaces of the pseudophakic eye. Average reproducibility for lens tilt and decentration of the phakic eye is 0.33 and 0.29 deg for horizontal and vertical tilt, respectively, and 0.03 and 0.02 mm for horizontal and vertical decentration, respectively. For the pseudophakic eye, average reproducibility for intraocular lens tilt is 0.55 and 0.6 deg for horizontal and vertical tilt, respectively, and 0.06 and 0.05 mm for horizontal and vertical decentration, respectively.

1. INTRODUCTION

Purkinje images are reflections of the light from anterior and posterior corneal surfaces (first and second Purkinje images, PI, PII although PII is difficult to image because it is overlaped by PI), and from anterior and posterior crystalline lens surfaces (third and fourth Purkinje images, PIII, PIV). They have been used for more than a century to assess properties of the cornea and crystalline lens. A more extensive historical background is provided in the introduction of this thesis. Purkinje images I, III and IV can be captured by imaging the eye's pupil, since they are formed within close distance of the pupillary plane (particulary PI and PIV). For example, for the Le Grand Model eye, for an object placed at 1 m, with a height of 18mm, the height of PIII relative to the height of the PI image is $\frac{h_3}{h_1} = 1.96$ and the height of PIV relative to the height of the PI image is $\frac{h_4}{h_1} = 0.76$. The position of the Purkinje images relative to the anterior cornea are 3.89 mm, 10.72 mm and 4.34 mm for PI, PIII and PIV, respectively. PI and PIV are relatively near to each other, so they are approximately in the same plane of focus, while PIII image is formed in a different plane.

Therefore, to visualize the three Purkinje images, the camera of a system for Purkinje image detection should be focused at different planes or a telecentric lens used to visualize the three Purkinje images in the same plane with the same magnification. Typically, illumination is performed off-axis to avoid overlapping of the images. In this thesis we developed a Purkinje-imaging based apparatus to measure the anterior and posterior radii of curvature and tilt and decentration of the crystalline lens or intraocular lenses in vivo. One of the earlier studies by Wulfeck (Wulfeck, 1955) described a system to image the third Purkinje Image using infrared photography, and established the basis of the current systems. Van Veen and Goss (Van Veen, 1988) presented a Purkinje Image system with a still flash camera. A similar system was used by Sorsby (Sorsby, Benjamin & Sheridan, 1961) in their studies correlating refractive error and geometrical properties of the ocular components. Mutti (Mutti, Zadnik & Adams, 1992) used a video camera for the first time and introduced a telecentric stop lens (which eliminates changes in magnification when an image is defocused) to record the three Purkinje images simultaneously (Zadnik, Mutti, Mitchell, Jones, Burr & Moeschberger, 2004).

Our phakometry system is based on previous developments by Smith and Garner (Smith & Garner, 1996) , the "Equivalent Mirror Theorem", and the method reported by Garner (Garner, 1997) based on an iterative method defining a "Merit Function". Lens tilt and decentration mesurements where obtained from equations presented by Phillips (Phillips, Perez-Emmanuelli, Rosskothen & Koester, 1988), that assume a linear relationship between Purkinje images positions and eye rotation, lens tilt and decentration.

Apart from phakometry, Purkinje images can also provide information on tilt and decentration of the ocular components and the lens in particular, which can be related to the optical quality of the eye. Several methodologies have been proposed to estimate lens tilt and decentration from Purkinje imaging systems. Several works, mainly from the clinical literature, estimate lens tilt by presenting to the subject fixation targets at different eccentricities and determining the fixation angle that produces an overlap of PIII and PIV (Guyton, Uozato & Wisnick, 1990). Phillips (Phillips et al., 1988) proposed a linear relation between Purkinje images locations and rotation of the eye, tilt and decentration of the lens in patients with IOLs. This methodology was validated and extensively used by Barry et al. in several studies of the misalignment of the ocular components (Barry, Branmann & Dunne, 1997, Barry, Dunne & Kirschkamp, 2001, Kirschkamp, Dunne & Barry, 2004).

Despite the fact that the use of Purkinje images to do phakometry and to measure tilt and decentration of the lens is well known, to our knowledge the description of the practical implementation of a compact system to measure both the normal lens and intraocular lens phakometry, tilt and decentration (in all orientations) has never been presented. In this thesis we designed a portable device to provide complete information of lens phakometry and positioning, and performed a thorough analysis of its performance through computational simulations (this Chapter) and validation experiments (Chapters 5 and 6).

In this chapter we present: 1) The design of the experimental set-up of a Purkinje imaging system. 2) A description of the algorithms developed to retrieve lens radii of curvature, lens tilt and decentration, and a comparison of the performance of the Equivalent Mirror and the Merit Function methods. 3) Computational validations of the measurements: The performance of the Equivalent mirror theorem and Merit function methods for phakometry has been assessed, in particular, the limitations that arise from considering paraxial optics, spherical surfaces, or constant refractive gradient index.

Models have been developed using real data obtained for individual eyes. The same eye models are used to evaluate the performance of Phillips' linear equations to obtain lens tilt and decentration. 4) First measurements of phakometry, lens tilt and decentration on young subjects with normal crystalline lens and on patients with IOLs.

This system, or slight modifications of it (adding a channel for central fixation or adding a mirror to reflect the fixation stimulus), was used in this thesis to: 1) Measure tilt and decentration in normal eyes and patients with intraocular lenses, presented in this chapter; 2) Compare phakometry measurements from Purkinje images and Scheimpflug imaging in the same set of phakic eyes (Chapter 5); 3) Compare tilt and decentration measurements from Purkinje and Scheimpflug imaging in a model eye, phakic and aphakic eyes (Chapter 6); 4) Compare measured and simulated aberrations in eyes with intraocular lenses, to identify the contribution of different factors, including IOL tilt and decentration, on optical quality degradation with cataract surgery (Chapter 9); 5) To evaluate the active or passive nature of the compensation of corneal coma by the crystalline lens, using pseudophakic eyes as a model (Chapter 10).

2. PURKINJE IMAGING

2.1 Optical Set up

Figure 2.1 and Figure 2.2 show, respectively, a schematic diagram and a photograph of the optical implementation of the Purkinje imaging set-up at the Visual Optics and Biophotonics Lab (Instituto de Optica, CSIC). The system is mounted on a 500 x 400 mm optical table. It has a symmetrical configuration for measurements on right and left eyes. The light sources are 880-nm LEDs (SFH485, Osram, 5-mm diameter, 22-deg emission angle; Maximum Radiant Intensity 80 mW/sr). Light from LED1 and LED2 is collimated by L1 and L2 (focal length= 125 mm, diameter= 12.5 mm). These channels illuminate the eye at an angle of 12 deg and are used for lens tilt/decentration measurements. Double LEDs (D-L1 and D-L2), separated by 18 mm and mounted at a distance of 65 mm from the eye at an angle of 15 deg were used to perform phakometry. The imaging channel consists of an IR-enhanced CCD camera (CV-M50IR, JAI) provided with a 55 mm focal length telecentric lens (Edmund Optics Ltd) mounted at a distance of 260 mm from the eye and focused at the pupil plane. This configuration resulted on a scale of 0.018 mm/pixel on the CCD chip. A third channel

projects a visual stimulus (FT) for foveal and eccentric fixations. It consists of a 12 x 9 mm minidisplay (Liteye Systems, pixel size 15x15μm), subtending a visual field of 7 deg, and a Badal system to correct for refractive errors and to meet different accommodation demands. The minidisplay has SVGA resolution and allows presentation of multiple targets. The Badal system consists of three lenses (L3 and L4 and L5, focal length=125 mm) allowing refractive corrections ranging from -8 to 8 D.

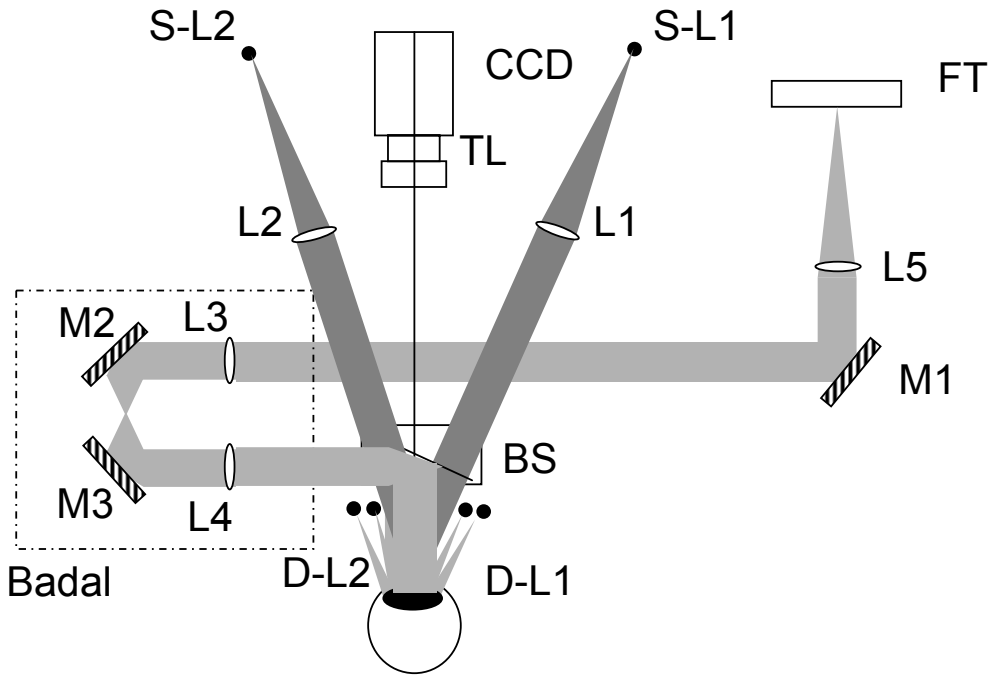

Figure 2.1. Diagram of the Purkinje Imaging system optical setup, with single LEDs (S-L1 and S-L2) collimated with achromatic lenses L1 and L2 (f=125 mm, ϕ = 25mm) for measurements of tilt and decentration on right and left eyes, and double LEDs (D-L1 and D-L2) for phakometry. Images are captured on a CCD camera with telecentric lens (TL). Fixation targets (FT) are presented on a minidisplay, collimated by L5 (f=125mm, ϕ = 38 mm) and inserted into the system with mirror M1. Illumination and imaging channels are separated by a hot mirror acting as a beam splitter (BS). A Badal system consisting of two mirrors (M2, M3) and three lenses (L3, L4 (f=125 mm, ϕ = 25mm), L5 (f=125 mm, ϕ = 38 mm)) allows for correction of refraction and for compliance of accommodative demands.

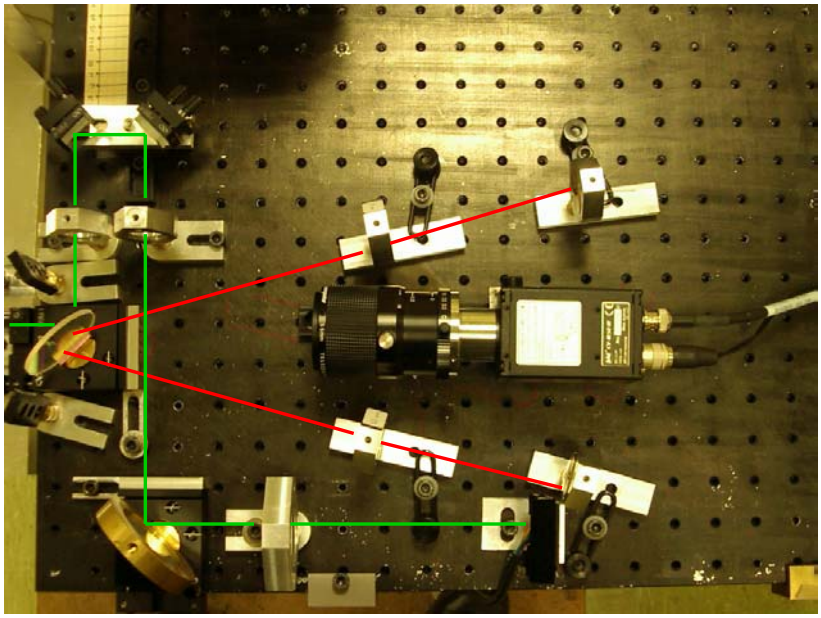

Figure 2.2. Physical set-up of the Purkinje imaging system

The system is controlled automatically with software written in Visual Basic (Microsoft Visual Studio, 6.0). The Windows-based program incorporates capture of pupillary images (by means of an acquisition board), presentation of targets on the system´s minidisplay (with a simultaneous view of the target on the controlling program), and patients data handling. For phakometry mesurements, the program controls the fixation target on the screen, so when the double Purkinje images are overlapped, the fixation target is moved until we obtain an image with separated Pukinje images. A screen capture of the software running the system is shown in Figure 2. 3.

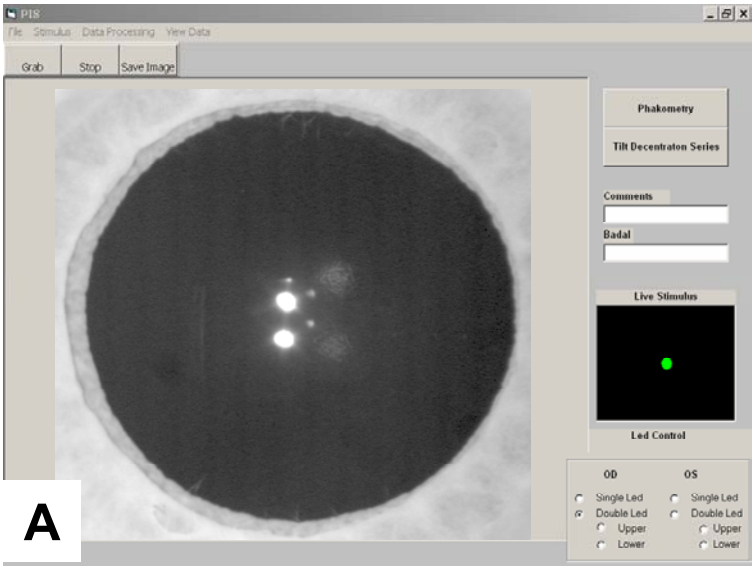

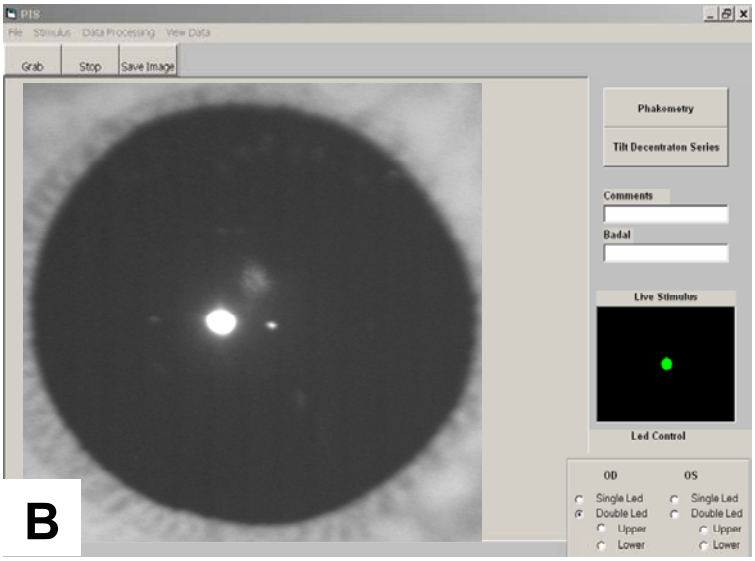

Figure 2.3.A. Image of the software running the system. Typical image of the phakometry mode. The software window contains a menu for file management, stimulus control, data processing. The pupilary image can be continuously viewed, sequences can be grabbed or images saved. **B.** Typical image of Tilt/Decentration mode. A live image of the stimulus viewed by the subject at each moment appears on the right bottom corner to the experimenter. For phakometry experiments, pushing the phakometry button activates the control of the fixation stimulus with the mouse that enables the shift of the fixation stimulus to different positions on the minidisplay. When the tilt and decentration button is clicked, the spot moves automatically to ten positions, for each of which pupilary images (such as that shown in 3.B. are grabbed). It is possible to save information about incidents during the measurement and about the Badal system in the comments and Badal boxes. Future control of the LEDs will be possible with the options that appear on the right bottom corner.

This system was modified to perform different studies. For a comparison to phakometry measurements with Scheimpflug imaging (Chapter 4), the Badal system was removed and a mirror was added. A channel for central illumination was inserted to obtain angle lambda to build a model eye to predict ocular aberrations after cataract surgery and to evaluate the compensation of spherical aberration and coma with aspheric IOLs (Chapter 9).

2.2 Purkinje image processing

We estimate the location of the Purkinje images referred to the pupil center. The center of the pupil is estimated by detection of the pupil margin which is fitted to a circle. The positions of the Purkinje images obtained from the reflection of the single

LED on the different ocular surfacesare detected through a Gaussian fitting with routines written in Matlab.

2.3 Phakometry

2.3.1. The Merit Function.

This is an iterative method, implemented by Garner (Garner, 1997), for calculation of the radius of curvature of both the anterior and posterior surfaces of the crystalline lens that can be applied to instruments with finite object distances, with objects of different heights and with stationary or mobile objects. For the context of this thesis, it will be used to the case of a stationary object.

The merit functions to evaluate are given by:

$$f_3 = \left[\left[\frac{h_3}{h_1}\right]_{theoretical}\right]^2 - \left[\left[\frac{h_3}{h_1}\right]_{\text{experimental}}\right]^2$$

$$f_4 = \left[\left[\frac{h_4}{h_1}\right]_{theoretical}\right]^2 - \left[\left[\frac{h_4}{h_1}\right]_{experimental}\right]^2 \qquad [2.1]$$

where $[h_3/h_1]_{\text{experimental}}$, $[h_4/h_1]_{\text{experimental}}$, are the experimentally obtained heights of PIII and PIV relative to PI, and $[h_3/h_1]_{\text{theoretical}}$, $[h_3/h_1]_{\text{theoretical}}$ are the height of PIII and PIV images relative to the height of PI, theoretically calculated from ray tracing. From initial values for the lens radius of curvature these are changed, until the merit function f_3 and f_4 reaches a minimum value.

To perform the ray tracing, the paraxial approximation is assumed and surfaces are considered to be spherical, therefore the image formed by refraction will be given by:

$$l'' = \frac{n_2 l r}{n_1 r + l(n_2 - n_1)}, \qquad [2.2]$$

Where l and l'' are the distances of the object in the object and image planes, respectively, n_1 and n_2 are the refractive index in the object and image space, respectively.

The reflected image can be found by substituting $n_2 = -n_1$ to obtain:

$$l'' = \frac{lr}{(2l - r)} \qquad [2.3]$$

The schematic eye used for ray tracing is given in Figure 2. 4.

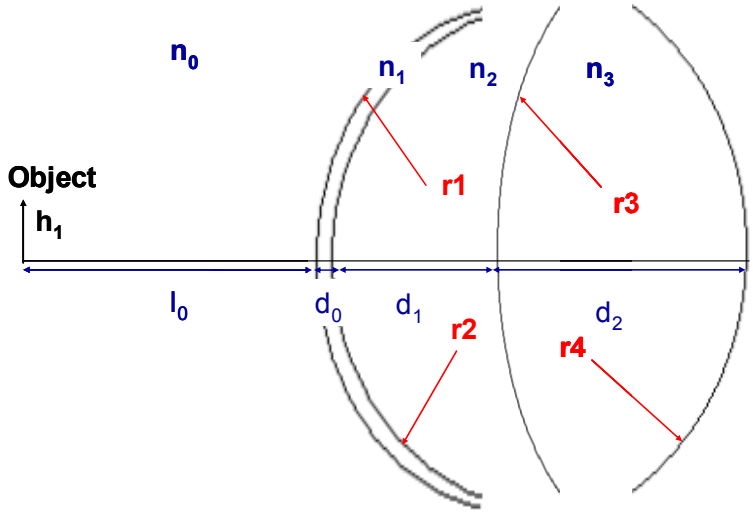

Figure 2.4. Schematic eye for paraxial ray tracing to obtain lens radius from the Merit Function.

r1, r2 are the anterior and posterior cornea radii of curvature, respectively, r3 and r4 are the anterior and posterior lens radii of curvature.

d_0= Corneal thickness, d_1 = Anterior chamber depth, d_2 = Lens thickness.

n_0 = Refractive index of the air, n_1 = Corneal refractive index, n_2 = Lens refractive index

The general paraxial equation:

$$\frac{n_2}{l''} - \frac{n_1}{l} = \frac{n_2 - n_1}{r}, \qquad [2.4]$$

can be written for refraction in the forms given by the equations 2.2 and 2.3.

The transverse magnification is given by:

$$M = -\frac{l''}{l} = \frac{r}{(r - 2l)} \qquad [2.5]$$

Where l and $l^{"}$ are as in equation 2.3.

Those equations will be applied for refraction and reflection from the different ocular surfaces.

2.3.1.1. First Purkinje image height:

Reflection in the anterior cornea:

After reflection, the position of PI relative to the anterior cornea will be given:

$$l_1^{"} = \frac{l_0 r_1}{(2l_0 - r_1)} \qquad [2.6]$$

Where l_0 and $l_1^{"}$ are the distance of the object to the anterior cornea and the first Purkinje image position, respectively, r_1 is the anterior corneal radius of curvature. Therefore, magnification of PI is:

$$M_1 = \frac{l_1^{"}}{l_0} \qquad [2.7]$$

and the height of PI is given by

$$h_1^{"} = M_1 h_1 \qquad [2.8]$$

Where h_1 is the object height.

2.3.1.2. Third double image height:

Refraction in the anterior cornea:

$$l_{3\_ant\_cornea} = \frac{n_1 l_0 r_1}{r_1 + l_0(n_1 - n_0)} \qquad [2.9]$$

Referred to the posterior cornea:

$$l_{3\_ant\_cornea}^{"} = l_{3\_ant\_cornea} - d_0 \qquad [2.10]$$

Refraction in the posterior cornea:

$$l_{3\_post\_cornea} = \frac{n_2 l'_{3\_ant\_cornea} r_2}{r_2 + l'_{3\_ost\_cornea}(n_2 - n_1)} \quad [2.11]$$

Referred to the anterior crystalline lens:

$$l''_{3\_ant\_crystalline} = l_{3\_post\_cornea} - d_1 \quad [2.12]$$

Reflection in the anterior crystalline lens:

$$l_{3\_ant\_crist} = \frac{-l''_{3\_post\_cornea} r_3}{r_3 - 2l''_{3\_post\_cornea}} \quad [2.13]$$

Here r_3 is the variable to evaluate in the Merit Function until a minimum is reached.

Referred to the posterior cornea:

$$l''_{3\_ant\_crist} = l_{3\_ant\_crist} + (d_1 - d_0) \quad [2.14]$$

Refraction in the posterior cornea:

$$l_{3\_post\_corn\_2} = \frac{n_1 l''_{3\_ant\_crist} r_2}{n_2 r_2 + l''_{3\_ant\_crist}(n_1 - n_2)} \quad [2.15]$$

Referred to the anterior cornea:

$$l''_{3\_post\_corn\_2} = l_{3\_post\_corn\_2} + d_0 \quad [2.16]$$

Refraction in the anterior cornea:

$$l_{3\_ant\_cornea\_2} = \frac{n_1 l''_{3\_post\_cornea\_2} r_1}{n_2 r_1 + l''_{3\_post\_cornea\_2}(n_1 - n_2)} \quad [2.17]$$

$l_{3\_ant\_cornea\_2} \equiv$ Position in z of PIII image referred to the anterior cornea.

Thus, magnification of PIII image would be:

$$M_3 = \frac{l_{3\_ant\_cornea} l_{3\_post\_cornea} l_{3\_ant\_cryst} l_{3\_post\_cornea\_2} l_{3\_ant\_cornea\_2}}{l''_{3\_ant\_cornea} l''_{3\_post\_cornea} l''_{3\_ant\_cryst} l''_{3\_post\_cornea\_2} l''_{3\_ant\_cornea\_2}} \quad [2.18]$$

Hence, the theoretical heights of PIII and PI are:

$$\left.\begin{array}{l} h_3'' = h_1 M_3 \\ h_1'' = h_1 M_1 \end{array}\right\} \Longrightarrow \frac{h_3''}{h_1''} = \frac{M_3}{M_1} \qquad [2.19]$$

To evaluate the Merit function for PIV, the same procedure is followed, taking into account refraction in the anterior lens and reflection in the posterior lens surface.

2.3.2. The Equivalent Mirror Theorem

Smith and Garner (Smith & Garner, 1996) proposed a method to calculate the lens radii of curvature using the equivalent mirror theorem that states that an optical system consisting of a number of refracting surfaces followed by a reflecting surface can be replaced by a single "equivalent mirror". The Equivalent Mirror Theorem states that the vertex and center of curvature of the equivalent mirror are conjugates of the vertex and centre of curvature of the real mirror, imaged by the refracting surfaces. If the target is at infinity, the image formed by reflection is proportional to the focal length of the surface, which is equal to one-half of the radius of curvature of the surface. Hence, the radius of curvature of the equivalent mirror, can be easily calculated from the expression:

$r_3'' = r_1 \left[\frac{h_3''}{h_1'} \right]$, where h_3'' and h_1'', the heights of PIII and PI.

For a practical configuration, it is better to place the light source near the eye to obtain brighter images. Also, as it has been addressed before, while PI and PIV images are formed in planes quite near to each other, PIII is formed in a different plane. Therefore focus should be adjusted to obtain a sharper PIII image. To overcome this problem, a telecentric lens is used, that allows to image PI, PIII and PIV Purkinje images (which will appeared out of focus) with the same magnification. Smith and Garner proposed methods to calculate the equivalent mirror radius of curvature in three cases:

a) The distance from the target to the corneal vertex is fixed, and the camera is focused on PI and then on PIII and PIV. b) The target is fixed to the camera, and the camera is focused on PI and then on the PIII image. c) The camera is focused on PI image, and only one recording is made. Thus, while PI will be sharp, PIII will be blurred, and it may lead to a measured image height that is different from the focused image.

For the purposes of this thesis, option a) has been used, and, since the camera used to visualize the three Purkinje images has a telecentric stop, refocus is not necessary. According to this, the scheme of the ray tracing procedure can be summarized in Figure 2. 5.

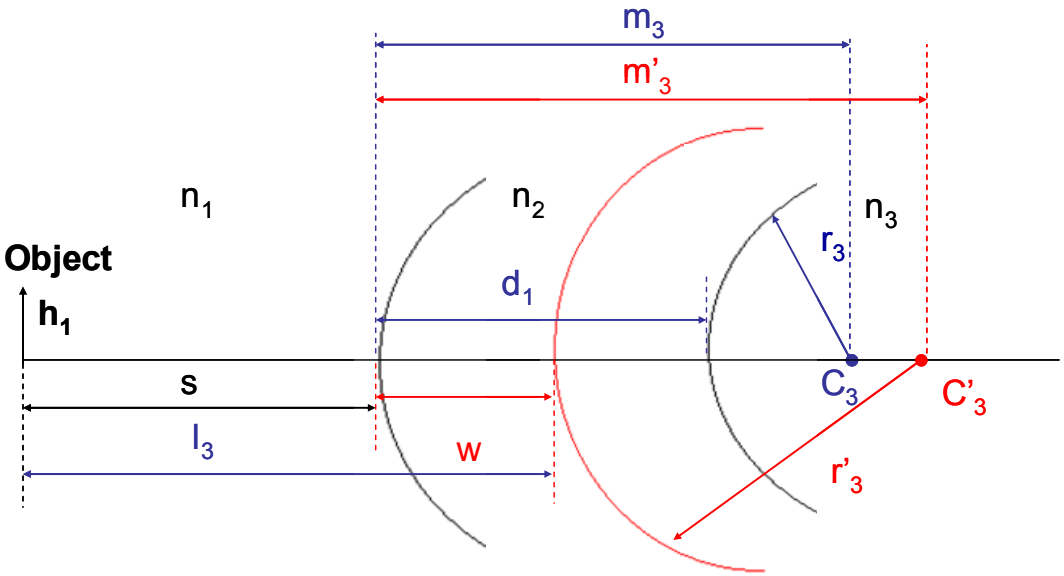

Figure 2.5. Schematic diagram for the Equivalent Mirror theorem

s is the distance of the object to the corneal vertex; l_3 is the distance of the object to the vertex of the Equivalent Mirror; w is the distance of the vertex of the anterior cornea to the vertex of the Equivalent Mirror; d_1 is the anterior Chamber depth; C_3 and C'_3 are the centers of curvature of the anterior lens and of the Equivalent Mirror for the anterior lens, respectively; r_3 and r_3'' are the radii of curvature of the anterior lens and of the Equivalent Mirror for the anterior lens, respectively; n_1, n_2, n_3, stand for the refractive index of air, cornea and lens respectively.

The radius of curvature r_3 of the anterior lens can be found using the equivalent mirror theorem by finding the positions of the vertex and centre of curvature of the equivalent mirror.

Considering that the refractive index in the object space is n_1 and the refractive index in the image space is n_2, applying equation 2.5.a, it follows that:

a) The distance w, distance from the image of the anterior surface of the lens to the corneal vertex, is given by:

$$w = \frac{n_1 d_1 r_1}{n_2 r_1 + d_1 (n_1 - n_2)} \qquad [2.20]$$

b) The distance $m_3^{"}$ from the corneal vertex to the center of curvature of the equivalent mirror is given by:

$$m_3^{"} = w + r_3^{"} \qquad [2.21]$$

where $r_3^{"}$ is the radius of the equivalent mirror.

Using equation 2.2 and given the same conditions for refractive index in image and object space, the position of the center of curvature of the anterior lens surface with respect to the corneal vertex is:

$$m_3 = \frac{n_2 m_3^{"} r_1}{n_1 r_1 + m_3^{"}\left(n_2 - n_1\right)} \qquad [2.22]$$

The equivalent anterior lens radius of curvature can be easily calculated:

The distance of the object to the corneal vertex is given by $l_1 = -s$, and the magnification after reflection in the anterior cornea is given by:

$$M_1 = \frac{h_1^{"}}{h_1} \qquad [2.23]$$

Magnification also can be expressed as:

$$M_1 = \frac{r_1}{\left(r_1 - 2l_1\right)} \qquad [2.24]$$

The vertex of the equivalent mirror is placed at $l_3 = -s - w$.

The magnification of PIII (from reflection of the "equivalent mirror" with an equivalent radius of curvature $r_3^{"}$) is given by:

$$M_3 = M_1\left[\frac{h_3^{"}}{h_1^{"}}\right], \qquad [2.25.a]$$

or alternatively by $M_3 = \frac{r_3^{"}}{\left(r_3^{"} - 2l_3\right)}$. [2.25.b]

From this expression, the radius of curvature of the equivalent mirror can be easily obtained:

$$r_3'' = \frac{2l_3 M_3}{(M_3 - 1)} \qquad [2.26]$$

With this expression for the radius of curvature of the equivalent mirror, the actual lens radius of curvature is given by:

$$r_3 = m_3 - d_1 \qquad [2.27]$$

The same procedure is followed to obtain the posterior lens radius of curvature.

In section 3.1 a computational study of the accuracy of the Equivalent Mirror and Merit Function methods will be presented. The assumptions made for the Merit Function are weaker than the used for the Equivalent Mirror Theorem, and can be applied under different conditions without change the procedure. Equivalent Mirror Theorem applied for finite targets, has been used in this thesis on a simpler three surfaces model eye, which can be the source of some inaccuracies although it could be used on a four surface model if the posterior corneal surface topography is known.

2.4 Lens tilt and decentration

The method to obtain lens tilt and decentration is based on that described by Phillips et al.(Phillips et al., 1988) and Barry et al. (Barry et al., 2001) in previous works. This method assumes a linear relation between Purkinje images positions and rotation of the eye, lens tilt and decentration.

$$\begin{aligned} P1 &= E\beta \\ P3 &= F\beta + A\alpha + Cd \\ P4 &= G\beta + B\alpha + Dd \end{aligned} \qquad [2.28]$$

where P1, P3 and P4 are the Purkinje images positions referred to the pupil center and β, α and d, are the rotation angle of the eye, tilt and decentration of the lens, respectively. These equations are applied to both horizontal and vertical coordinates.

To obtain the coefficients in these equations for each eye, we resort to simulated model eyes with spherical surfaces and the individual parameters available for each subject, using an optical design program (Zemax, Focus Software). The anterior corneal radius of curvature and anterior chamber depth were obtained from optical biometry, and anterior and posterior lens radii of curvatures were obtained from the phakometry

measurements. Corneal thickness, lens thickness and lens refractive index were taken as constant in all eyes, using data from the unaccommodated Gullstrand model eye. IOL parameters were obtained from published data on these lenses (Sverker, Artal, Piers, Mooren & et al, 2003) or data provided by the manufacturer. Indices of refraction for the wavelength of illumination were used, using conversion factors reported by the Herzberger formula (Herzberger, 1969) given by equation 2.31.

$$n = a + bL + cL^2 + d\lambda^2 + e\lambda^4 + f\lambda^6 \qquad [2.29]$$

with $L = \frac{1}{\lambda^2 - 0.028}$ and *a, b, c, d, e, f* being the dispersion coefficient data of the corresponding media provided by Zemax.

The optical surfaces were assumed to be spherical, although validations of the technique were performed incorporating aspheric surfaces, actual corneal topographies and gradient index of refraction into the models.

To obtain coefficients *E, F* and *G*, α and *d* are set to zero (no tilt and no decentration) in the model. We estimated the Purkinje images positions in equation [2.28] for different rotation angles, and calculated coefficients *E, F, G* by linear fitting of the slope. The same procedure was repeated for *A* and *B* (setting $\beta = 0$ and $d = 0$) and *C* and *D* (with $\beta = 0$ and $\alpha = 0$).

The rotation angle (β), tilt (α) and decentration of the lens (d) can then be solved using the individual coefficients for each eye and the experimental Purkinje image locations (P1, P3 and P4):

$$\begin{aligned} \beta &= \frac{P1}{E} \\ \alpha &= \frac{\left[\beta(DF - CG) + CP4 - DP3\right]}{\left[CB - DA\right]} \\ d &= \frac{\left[P3 - \beta F - \alpha A\right]}{C} \end{aligned} \qquad [2.30]$$

The procedure is done for both horizontal and vertical coordinates.

Horizontal tilt refers to tilt around y-axis and vertical tilt refers to tilt around the x-axis. Positive tilt around the horizontal axis (α_x) means that the superior edge of the lens moves closer to the cornea than the inferior edge, and vice versa for negative.

Positive tilt around the vertical axis (α_y) means that the nasal edge of the right lens or the temporal edge of the left lens moves backwards, and vice versa for negative.

Positive horizontal decentration (d_x) means that the right lens is shifted toward the nasal side or that the left lens is shifted towards the temporal side and vice versa for negative. Positive vertical decentration (d_y) indicates that the lens is shifted upwards and vice versa for negative. A scheme of the sign criteria for lens tilt and decentration is presented in Figure 2.6.

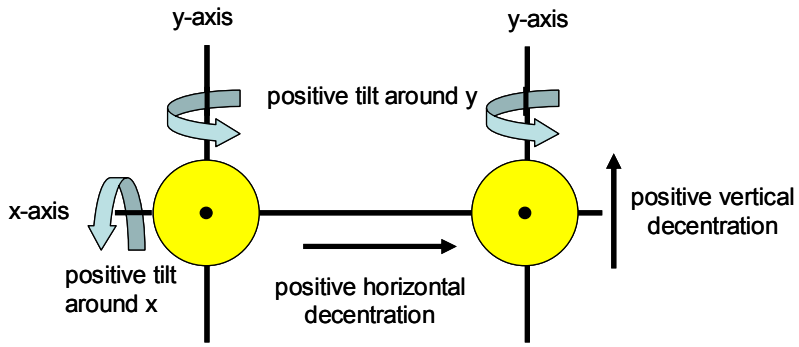

Figure 2.6. Scheme of the sign convention for lens tilt and decentration measurements as seen by the observer.

3. VALIDATION OF THE TECHNIQUE BY COMPUTER SIMULATIONS

We performed computer simulations to test individually the validity of the assumptions involved in the described procedures. Additionally, measurements in patients with IOLs allowed us to perform comparisons with nominal values and comparisons with other methods.

3.1 Test of Purkine phakometry methods using computer eye models

We performed computer simulations to test the performance of the Equivalent Mirror and Merit function approaches to obtain phakometry. Simulations are based on the same simplified eye model (spherical surfaces, constant refractive index) as the model that we used in the processing algorithms. Table 1 shows the parameters of the eye model used in the simulation, as well as the individual parameter that was varied in each case to test separately the impact of each of the assumptions. All simulations were performed in Zemax, using the actual experimental conditions for illumination (double LED, distance from the LED to the eye, and angle of illumination). The actual images

of PI, PIII and PIV were obtained by using ray tracing and intensity distribution analysis in Zemax. Figure 2.7 shows the retrieved Purkinje images positions from simulations in Zemax. As in the experiments, the locations of the double Purkinje images of PI, PIII and PIV were obtained by fitting Gaussian functions to the images. From those locations, we computed the relative heights. We used these values in the same algorithms that processed our experimental data and compared the resultant radii of curvature with the nominal values from the eye model. Table 1 shows the retrieved anterior and posterior lens radii of curvature for different combinations of anterior and posterior nominal lens radii of curvature in the model eye. For eyes with anterior lens radii ranging from 14 to 10 mm we found average discrepancies of 0.09 mm for the anterior lens and 1.12 mm for the posterior lens with the equivalent mirror method and 0.09 mm for the anterior lens and 0.33 mm for the posterior lens with the Merit function method. For eyes with posterior lens radii ranging from -4 to -6 mm, we found average discrepancies of 1.06 mm and 0.30 mm in the retrieved posterior lens radius of curvature with the merit function and equivalent mirror methods, respectively**.**

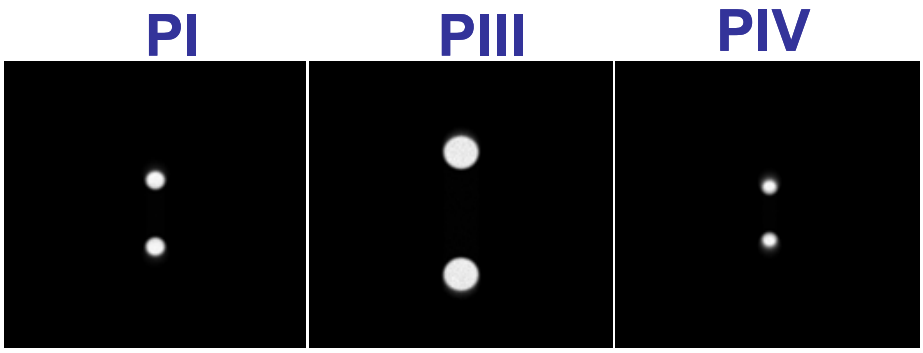

Figure 2.7. Example of simulated Purkinje images for phakometry evaluation, using Zemax.

Alternatively, we compared the experimental heights of the Purkinje images with those obtained through simulations in Zemax using the experimentally retrieved values of anterior and posterior lens radii of curvatures. We found average discrepancies of 0.009 mm for h_1, 0.131 mm for h_3, and 0.002 mm for h_4. The discrepancies in Purkinje images heights obtained experimentally and with simulations in Zemax, translated into radii of curvature differences of 0.366 mm and 0.075mm for the anterior lens (with the Equivalent Mirror method and the Merit function respectively) and 1.09 mm and 0.217 mm for the posterior lens. These discrepancies in h_1, h_3 and h_4 are close to the

distance measurement accuracy (taking into account that pixel resolution is 0.08 mm at the pupil plane).

We also performed simulations to assess the influence of possible tilt and decentration of the lens, corneal curvature, anterior chamber depth and lens thickness on the phakometry measurements.

3.1.1. Effect of lens tilt and decentration.

To evaluate possible effects of misalignment of the lens on the estimates of lens radii of curvature we simulated the same model eye with the parameters shown in Table 1, and a decentered and tilted lens. We obtained a discrepancy of 0.28 mm for the anterior lens and 1.55 mm for the posterior lens using the Equivalent Mirror method, and 0.66 mm for the anterior lens and 0.46mm for the posterior lens with the merit function method.

3.1.2. Effect of anterior and posterior corneal curvature.

We checked that the estimates were not affected by the nominal corneal curvatures. The anterior corneal radius of curvature was changed in the processing algorithm according to the nominal value of the model, while the posterior corneal radius of curvature was kept constant in the processing algorithm. For the values of the eye model shown in Table 1, and varying the anterior corneal curvature, we found average discrepancies of 0.12 and 0.29 mm for the retrieved anterior lens radius of curvature, and 1.02 and 0.21 mm and for the retrieved posterior lens radius of curvature, using the Equivalent Mirror and the Merit function methods respectively**.** For the fixed values of the model shown in Table 1, and varying the posterior corneal curvature, we found average discrepancies of 0.43 and 0.29 mm in the retrieved anterior lens radius of curvature with the Equivalent Mirror and Merit function methods respectively. For the posterior lens radius of curvature we found discrepancies of 1.14 and 0.16 mm with the Equivalent Mirror Theorem and Merit Function respectively**.**

3.1.3. Effect of Anterior Chamber depth.

When the anterior chamber depth was varied in a range consistent with values measured in real eyes (see Table 1), we found average discrepancies of 0.24 and 0.19 mm for the retrieved anterior lens radius of curvature, and of 1.33 and 0.33 mm for the

retrieved posterior lens radius of curvature, using the Equivalent Mirror and Merit function methods respectively. Additionally, we tested that discrepancies of 0.5 mm between the anterior chamber depth used in the model eye and that used in the simulation produced average discrepancies of 0.4 and 0.026 mm for the retrieved anterior lens radius of curvature, and of 1.46 and 0.41 mm for the retrieved posterior lens radius of curvature, with the Equivalent Mirror and Merit Function methods, respectively.

3.1.4. Effect of lens thickness.

We tested the effect of the assumption of a constant value for lens thickness, changing this parameter in the model eye (see Table 1) while keeping it constant in the processing algorithms. We found that discrepancies of 0.5 mm between the lens thickness value used in the model eye and that used in the simulation produced average discrepancies of 0.36 and 0.56 mm for the retrieved posterior lens radius of curvature with the equivalent mirror and merit function methods, respectively**.**

In summary, for the anterior lens radius of curvature, both methods work theoretically within accuracies <0.3 mm, and for the posterior lens the accuracies are within 1 mm for the Equivalent Mirror and 0.3 mm for the Merit function. The estimates are not significantly affected by the assumptions regarding posterior corneal radius of curvature and lens thickness, in particular when using the Merit function method.

In brief, these simulations show that, assuming spherical surfaces and for the experimental conditions of the system, the Merit Function provides accurate estimates of phakometry, while the Equivalent Mirror slightly overestimates the posterior lens radius of curvature for this model eye.

3.2 Test of lens tilt/decentratrion methods using computer eye models

We performed computer simulations to check the accuracy of the Phillips Equations retrieving tilts and decentrations. We built a computer model eye with nominal values as in Table 1 (row 7), imposing crystalline lens tilts and decentrations. Different combinations of tilt and decentrations were also tested (with eye rotations up to 3.5 deg,

lens tilts up to 5 deg and decentrations up to 0.25 mm). We estimated the coefficients of Eq. (2.28) for the model eye as described in subsection 3.1 for real eyes. Intensity distributions for Purkinje images PI, PIII and PIV were simulated as described above, for the actual experimental conditions of eye rotation and angle of illumination, and P1, P3 and P4 in Eq. (2.28) were estimated as in the experimental images. Eye rotation, lens tilt and decentration were obtained, as described for real eyes, by using Eq. (2.32). We found maximum discrepancies of 0.1 deg in eye rotation, 0.6 deg in lens tilt and 0.026 mm in decentration.

Using similar procedures, we simulated P1, P3 and P4 for measured values of anterior corneal radii of curvature, anterior and posterior crystalline lens radii of curvature, and anterior chamber depth in one of the measured patients and compared experimental locations of the Purkinje images with the predictions from Zemax. We found average discrepancies of 0.058 mm for P1 in the horizontal direction and 0.024 mm in the vertical direction, 0.024 mm for P3 in the horizontal direction and 0.03mm in the vertical direction, and 0.058 mm for P4 in the horizontal direction and 0.02 mm in the vertical direction.

Finally, we tested that discrepancies of 1 mm in the estimated anterior and posterior radii of curvature produced discrepancies of less than 0.2 deg in the tilt estimates and 0.01 mm in the decentration estimates.

3.3 Test of the validity of the assumptions in the model eye

The computer simulations presented in Table 1 were aimed at testing the validity of the procedures with the actual experimental conditions, but used simplified eye models with spherical surfaces and constant refractive index. We have performed additional simulations to test the impact of these assumptions on the estimated lens radii of curvature and lens tilt and decentration. The parameters of the model in each condition and the results are presented in Table 2. Purkinje images were simulated by using more realistic eye models, while phakometry and lens tilt and decentrations were obtained by using the same routines as those in previous simulations and in the experiments. Implicitly these tests also checked the validity of the paraxial approximation.

3.3.1. Effect of anterior corneal asphericity.

We assumed the same eye model than in previous simulations, but with anterior corneal conic constants consistent with reports from Dubbelman (Dubbelman, Weeber,

van der Heijde & Volker-Dieben, 2002) (see Table 2). The retrieved anterior lens radii differed from nominal values by 0.09 and 0.35 mm with the equivalent mirror and merit function methods, respectively, and the posterior lens radii differed by 0.94 and 0.13 mm, respectively**.**

3.3.2. Effect of corneal irregularities.

We replaced the theoretical cornea in the model eye by the corneal elevation map obtained with the corneal topographer in two real eyes (fit to a seventh order Zernike polynomial and described in Table 2 in terms of third and higher root-mean-square errors, excluding spherical terms). We found average discrepancies of 0.59 and 0.15 mm for the retrieved anterior lens radius of curvature and 0.9 and 0.35 mm for the retrieved posterior lens radius of curvature, using the Equivalent Mirror and Merit function methods, respectively.

3.3.3. Effect of anterior and posterior lens asphericities.

We used the same eye model as that in previous simulations but assuming lens asphericities consistent with reports from Dubbelman (Dubbelman & van der Heijde, 2001), as shown in Table 2. When the lens anterior surface asphericity was varied, we found that the estimates of anterior lens radii are only slightly affected by changes in anterior lens asphericity (average discrepancies of 0.54 and 0.16 mm with the equivalent mirror and merit function methods respectively), but that discrepancies in posterior lens radii are higher (average discrepancies of 2.19 and 0.98 mm, with the equivalent mirror and merit function methods respectively)**.** The average discrepancies in the posterior lens radii (changing the posterior lens asphericity) were 2.3 and 1.07 mm, with the Equivalent Mirror and Merit Function methods, respectively. These simulations show that the Merit Function Method is more robust to the presence of aspheric surfaces and provides significantly better results than does the equivalent mirror method.

3.3.4. Effect of refractive gradient index in a realistic eye model.

Finally, we tested the accuracy of the phakometry methods and tilt/decentration estimates using the realistic eye model described in Table 2, rows 12-13. This included real anterior corneal elevation from corneal topography, aspheric posterior corneal surfaces, anterior and posterior aspheric lens surfaces, and, particularly, a gradient index distribution for the crystalline lens (based on the model proposed by Garner and Smith

(Garner & Smith, 1997)). With this model eye, we found a discrepancy of 0.85 and 0.66 mm for the retrieved anterior lens radius of curvature, and of 1.35 and 0.75 mm for the retrieved posterior lens radius of curvature with the equivalent mirror and merit function methods, respectively. These values are only slightly higher than the discrepancies obtained using the same eye model (with spherical surfaces and constant index of refraction) in the simulations and in the reconstructions algorithms.

We also checked that the approximations of the model did not affect the results of lens tilt and decentration. The coefficients in Phillips' equation changed by 8% on average between using the spherical model eye and the more realistic model eyes described above. These discrepancies produced differences between the estimates lower than 0.09 and 0.01 deg for horizontal and vertical tilt, and lower than 0.16 and 0.02 for horizontal and vertical decentration, respectively, for the same nominal tilts and decentrations as those used in 3.2. Finally using the same procedures described in 3.1.3 we simulated Purkinje images for a given tilt and decentration of the crystalline lens, in the realistic eye model described above, and compared the nominal values with those obtained with the algorithms. We found maximum discrepancies of 0.1 deg in eye rotation, 0.25 deg in lens tilt and 0.013 mm in decentration. Those discrepancies are comparable to those obtained in section 3.2 where the simulations were performed using the same eye model than the processing algorithms, considering spherical surfaces used in the algorithms.

Table 2.1. Model Eye with spherical surfaces; n_{cornea}=1.3687; n_{lens}=1.41; n_{aquous}=1.32854, for 880 nm in Zemax with Herzberger formula

Eye Model Nominal Values								*Retrieved values*			
								Equivalent Mirror		*Merit function*	
Anterior corneal radius (mm)	**Posterior corneal radius (mm)**	**Anterior chamber depth (mm)**	**Lens thickness (mm)**	**Lens decentration (mm)**	**Lens tilt (deg)**	**Anterior lens radius (mm)**	**Posterior lens radius (mm)**	**Anterior lens radius (mm)**	**Posterior lens Radius (mm)**	**Anterior lens radius (mm)**	**Posterior lens radius (mm)**
7.73	6.5	3.61	4	0	0	**10**	-6	10.15	-7.35	9.96	-6.51
7.73	6.5	3.61	4	0	0	**12**	-6	12.13	-7.04	11.94	-6.27
7.73	6.5	3.61	4	0	0	**14**	-6	13.99	-7.35	13.80	-6.53
7.73	6.5	3.61	4	0	0	10.45	**-6**	10.68	-7.12	10.32	-6.15
7.73	6.5	3.61	4	0	0	10.45	**-5**	10.68	-6.03	10.32	-5.28
7.73	6.5	3.61	4	0	0	10.45	**-4**	10.68	-5.06	10.32	-4.48
7.73	6.5	3.61	4	**1**	**5**	10.45	-6	10.18	-7.55	9.79	-6.46
8.5	6.5	3.61	4	0	0	10.45	-6	10.49	-7.03	10.23	-6.19
7.5	6.5	3.61	4	0	0	10.45	-6	10.55	-7.16	10.14	-6.14
6.5	6.5	3.61	4	0	0	10.45	-6	10.69	-6.88	10.08	5.69
7.73	**6.5**	3.61	4	0	0	10.45	-6	10.56	-7.24	10.19	-6.24
7.73	**6**	3.61	4	0	0	10.45	-6	10.57	-7.21	10.19	-6.22
7.73	**5.5**	3.61	4	0	0	10.45	-6	10.48	-6.97	10.11	-6.03
7.73	6.5	**4**	**4**	0	0	10.45	-6	10.92	-7.52	10.54	-6.47
7.73	6.5	**3.5**	**4**	0	0	10.45	-6	10.58	-7.27	10.21	-6.27
7.73	6.5	**2**	**4**	0	0	10.45	-6	10.57	-7.19	10.19	-6.26
7.73	6.5	3.61	**3**	0	0	10.45	-6	10.7	-5.91	10.84	-5.17
7.73	6.5	3.61	**3.5**	0	0	10.45	-6	10.7	-6.64	10.84	-5.75
7.73	6.5	3.61	**4**	0	0	10.45	-6	10.7	-6.97	10.84	-6

Table 2.2. Model eye with aspheric surfaces, real corneal topography and/or GRIN

1) Asphericity defined for this surface: $h^2 + (1+Q)Z^2 - 2ZR = 0$ where the Z axis is the optical axis, $h^2 = X^2 + Y^2$, R is the vertex radius of curvature and Q is the surface asphericity.

2) 3rd order and higher corneal surface RMS (fitted to a seventh- order Zernike polynomial), without spherical terms c12 and c24.

3) Gradient index profile in the equatorial plane defined by Garner (Garner & Smith, 1997): $n(y) = n_c + c_1\left(\frac{y}{b}\right)^2$ where $n_c = 1.406$ refractive index in the center of the lens, b is the equatorial radius and c_1 is the CRIN shape distribution inside the lens.

Eye Model Nominal Values													***Retrieved values***			
													Equivalent Mirror		***Merit function***	
Anterior corneal			**Posterior cornea**		**Anterior lens**		**Lens**				**Posterior lens**		**Anterior lens radius (mm)**	**Posterior lens Radius (mm)**	**Anterior lens radius (mm)**	**Posterior lens radius (mm)**
Radius (mm)	**Aspher.[1]**	**RMS[2]**	**Radius (mm)**	**Aspher**	**Radius (mm)**	**Aspher**	**Refractive Index (IR) [3]**		**Tilt**	**Dec en.**	**Radius (mm)**	**Aspher**				
							const	**Grad (equ. index)**								
7.73	**-0.5**	0	6.5	-0.28	10.45	0	1.41	0	0	0	-6	0	10.39	-6.99	10.03	-6.04
7.73	**-0.3**	0	6.5	-0.28	10.45	0	1.41	0	0	0	-6	0	10.39	-7.06	10.03	-6.10
7.73	**-0.2**	0	6.5	-0.28	10.45	0	1.41	0	0	0	-6	0	10.61	-7.37	10.24	-6.34
7.73	-	0.84	6.5	-0.28	10.28	0	1.41	0	0	0	-6.53	0	10.82	-7.11	10.45	-6.14
7.84	-	0.42	6.5	-0.28	11.95	0	1.41	0	0	0	-5.75	0	11.32	-6.97	11.82	-6.04
7.73	0	0	6.5	0	10.45	**-5**	1.41	0	0	0	-6	-3.25	11.14	-8.25	10.76	-7.03
7.73	0	0	6.5	0	10.45	**-3**	1.41	0	0	0	-6	-3.25	10.94	-8.28	10.56	-7.05
7.73	0	0	6.5	0	10.45	**-2**	1.41	0	0	0	-6	-3.25	10.89	-8.06	10.52	-6.88
7.73	0	0	6.5	0	10.45	-4.25	1.41	0	0	0	-6	**-3**	11.28	-8.3	10.89	-7.07
7.73	0	0	6.5	0	10.45	-4.25	1.41	0	0	0	-6	**-2**	11.28	-7.72	10.89	-6.62
7.73	0	0	6.5	0	10.45	-4.25	1.41	0	0	0	-6	**-1**	11.28	-7.51	10.89	-6.46
7.73	-	0.84	6.5	-0.28	10.28	-4.25	0	1.425	0	0	-6.53	-3.25	12.59	-8.25	10.93	-7
7.84	-	0.42	6.5	-0.28	11.95	-4.25	0	1.419	0	0	-5.75	-3.25	13	-7.84	12.59	-6.69
7.73	-	0.84	6.5	-0.28	10.28	-4.25	0	1.425	**5**	**1**	-6.53	-3.25	11.53	-8.06	11.12	-6.86

4. PRELIMINARY TESTS IN PHAKIC AND PSEUDOPHAKIC EYES

4.1 Data acquisition

Subjects are aligned to the system while looking foveally at a fixation crosstarget presented on the minidisplay. The subject´s pupil is aligned to the optical axis of the CCD camera while moving the subject´s head on a X-Y-Z stage. The subject´s head is stabilized by means of a dental impression. Spherical refractive error was corrected with the Badal system which was set in the position for which the subject reported that the stimulus looked sharpest. In subjects with accommodative capability, special care was taken to ensure that the eye was not accommodating. Measurements were typically done under normal viewing conditions in the young eyes and mydriasis (tropicamide 1%) in patients with IOLs.

A set of pupillary images showing PI, PIII and PIV are captured, with SL1 (for OD) or SL2 (for OS) on, for ten different fixations on the minidisplay (green spots on a black background). Fixation locations ranged from +3.5 to -3.5 deg in the horizontal direction, and from +2.5 to -2.5 deg in the vertical direction. These images were used for estimations of lens tilt and decentration. We captured three sets of images for statistical purposes.

Pupillary images showing double PI, PIII and PIV were also captured with D-LED1 (for OD) or D-LED2 (for OS) on, with the patient fixating foveally. Occasionally, the fixation target had to be moved off-axis to allow proper visualization of the images (a special module in the software allows easy shift and documentation of the fixation location). These images were used for estimations of lens radii of curvature. We captured three sets of images (for vertical and horizontal directions) for statistical purposes. Additional measurements on the subjects included corneal topography (Atlas, Humphrey Instruments) axial length, anterior chamber depth and keratometry (IOL Master, Zeiss), and autorefraction (Automatic Refractor Model 597, Zeiss). IR (780 nm) retro-illumination images (from a pupil imaging channel in the Laser Ray Tracing system developed in our laboratory (Llorente, Barbero, Cano, Dorronsoro & Marcos, 2004) were also captured in patients with implanted IOLs. Figure 2.8 shows typical images for phakometry obtained in normal eyes and patients with IOLs. Figure 2.9 shows typical images used to estimate tilt and decentration in normal eyes and in patients with IOLs.

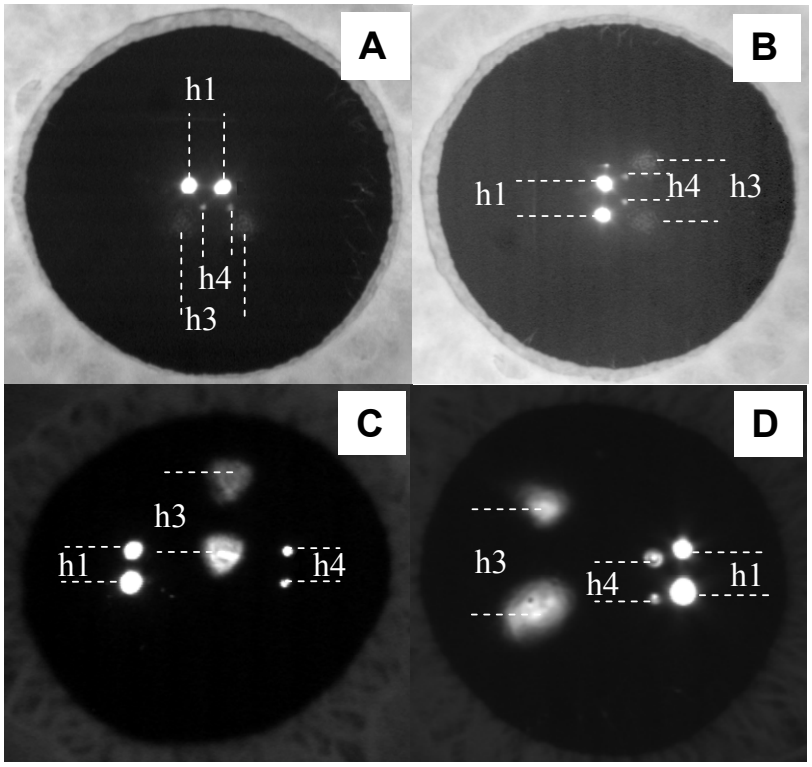

Figure 2.8. Examples of pupillary images showing double PI, PIII and PIV used to obtain phakometry. **A.** Eye with normal crystalline lens (eye #1, OD), in the horizontal direction. **B.** Eye with normal crystalline lens (eye #1, OD), in the vertical direction. **C.** Eye with IOL (eye #2, OS). **D.** Eye with IOL (eye #2, OS).

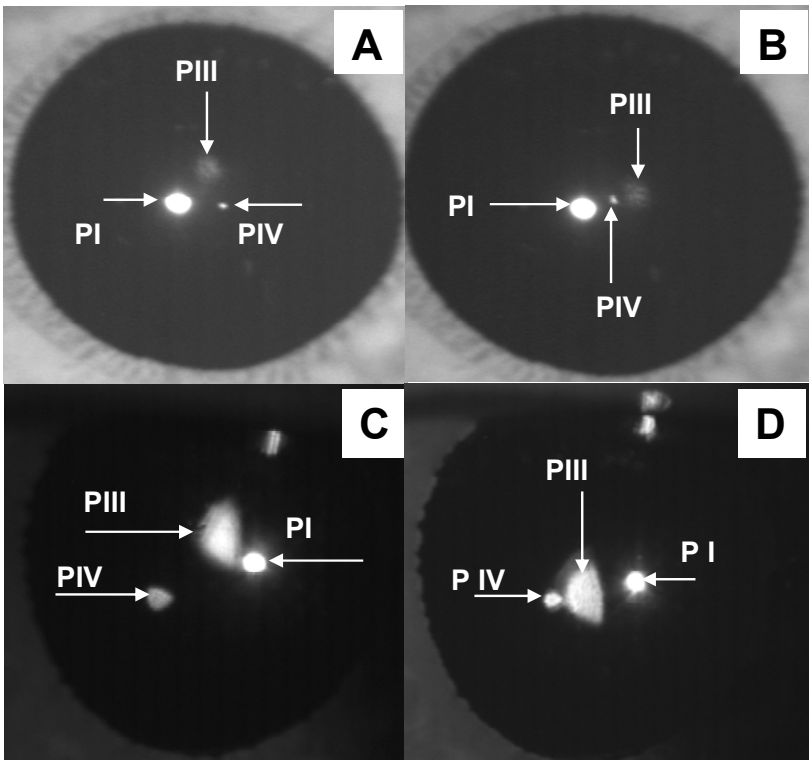

Figure 2.9. Examples of pupillary images showing PI, PIII and PIV used to obtain tilt and decentration, for different fixation angles. **A.** Eye with normal crystalline lens (subject #15, OD) fixating at -3.5 deg temporal. **B.** Eye with normal crystalline lens (subject #15, OD) fixating at 3.5 deg inferior **C.** Eye with IOL (eye #2, OS) fixating at 1.7deg superior. **D.** Eye with IOL (eye #2, OS) fixating at 1.7 deg inferior.

4.2 Subjects

Measurements were made on 17 eyes from normal subjects, moderately myopic with spherical errors ranging from 1.25 to -7 D (mean= -1.71±2.39 D) and ages ranging from 24 to 30 years (mean= 26.67±2.31 yr). Additionally, in this preliminary study, we measured nine eyes of five subjects implanted with IOLs (with both aspheric and spherical designs), with ages ranging from 71 to 79 years (mean=74±2.3 yr.). All subjects were informed of the nature of the study before the experiments and signed a consent form. The study followed the tenets of the declaration of Helsinki.

4.3 Results of phakometry measurements in young eyes and on eyes of patients with IOLs

Figure 2.9 shows the anterior and posterior radii of curvature for 12 young subjects. Radii of curvature of the anterior lens surface ranged from 8.81 ± 0.21 to 12.69± 0.37 mm, and radii of curvature of the posterior lens ranged from -7.09 ± 0.41 to -5.64 ± 0.44 mm, with use of the merit function method. The equivalent mirror method yielded similar radii for the anterior lens (ranging from 8.83 ± 0.39 to 12.86 ± 0.38) mm, and slightly values for the posterior lens (ranging from -8.43 ± 0.66 to -6.47± 0.16) mm, consistent with the predictions from the simulations.

We measured radii of curvature in the vertical and in the horizontal directions in five subjects. Differences across meridians were not significant, except for two subjects, where we found differences of 0.82 mm for the anterior lens and 0.84 mm for the posterior lens across meridians. Reproducibility of the measurements are 0.34 and 0.28 mm for the anterior and posterior lens radius of curvature respectively.

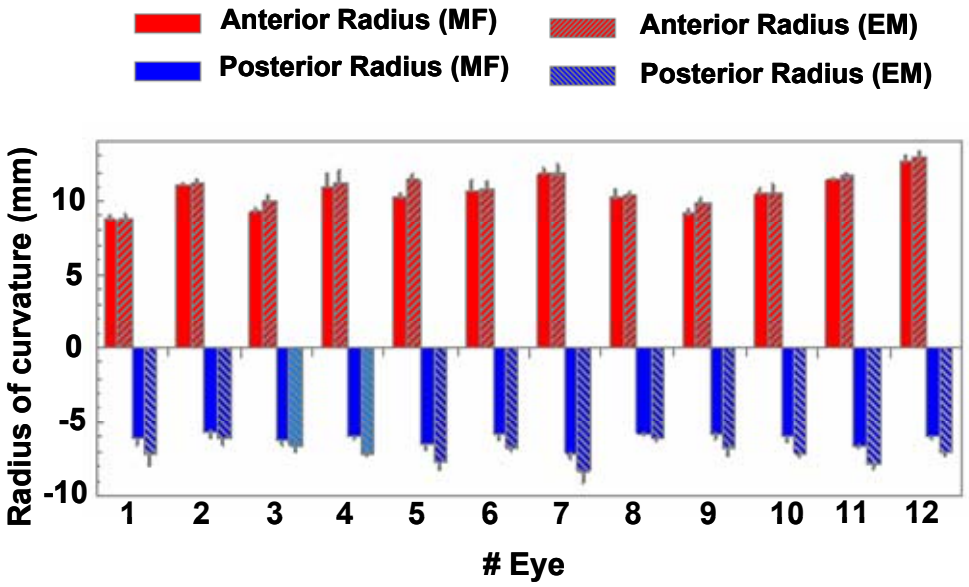

Figure 2.10. Anterior and posterior radii of curvature, estimated using the Merit function (MF) and the Equivalent Mirror (EM) methods. Eyes (right eyes from 12 subjects) are ranked by increased myopic error. Values are average of at least three measurements. Error bars stand for standard deviations.

4.4 Crystalline Lens tilt and decentration

Figure 2.11.A shows horizontal and vertical crystalline lens tilt, and Figure 2.12.B shows horizontal and vertical crystalline lens decentration on 17 eyes of 14 subjects. Solid symbols stand for right eyes and open symbols stand for left eyes.

Horizontal tilt ranged from -1.13 ± 0.43 to 2.8 ± 0.40 deg in right eyes and from -1.96 ± 0.36 to -2.87 ± 0.34 deg in left eyes. Vertical tilt ranged from –1 ± 0.31 to 2.58± 0.27 deg in right eyes, and from 0.66 ± 0.20 to 1.99 ± 0.43 deg in left eyes. Crystalline lens tilt tended to be mirror-symmetric in left/right eyes of the same subject. Crystalline lens decentrations ranged, in the horizontal direction, from -0.098 ± 0.031 to 0.445 ± 0.023 mm in right eyes and -0.36 ± 0.013 to 0.39 ± 0.032 mm in left eyes. Vertical decentrations ranged from -0.22 ± 0.02 to 0.04 ± 0.02 mm in right eyes and from -0.18 ± 0.003 to 0.06 ± 0.01 mm in left eyes. Reproducibility of the measurements are 0.29 deg and 0.33 deg for horizontal and vertical tilt, and 0.03 mm and 0.02 mm for horizontal and vertical decentration.

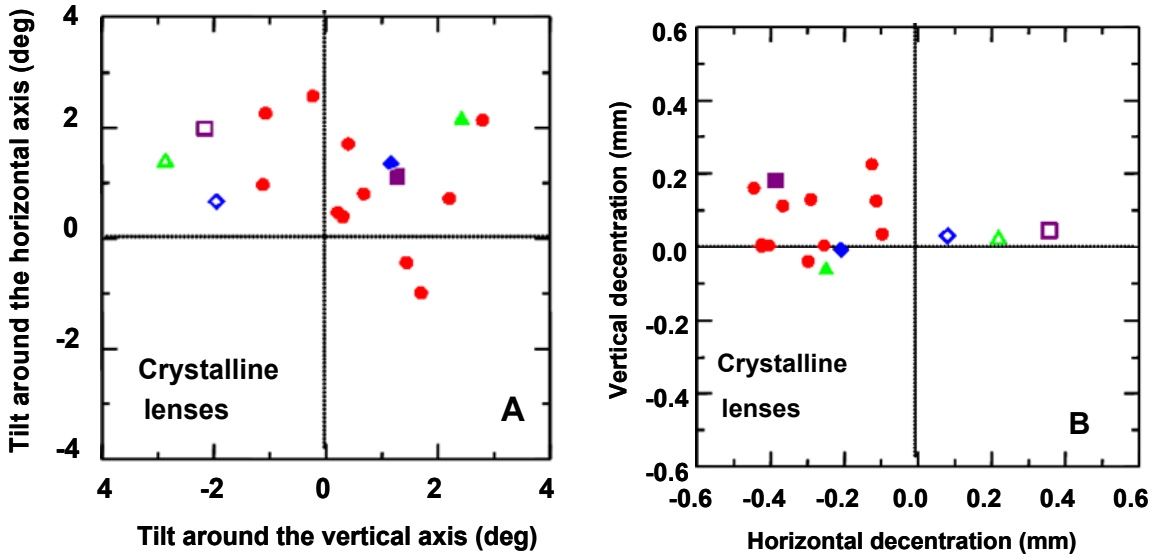

Figure 2.11. A. Tilt around the horizontal and vertical axis of the crystalline lens in 17 eyes of 14 subjects. Solid symbols correspond to right eyes, and open symbols to left eyes. Circles correspond to subjects 1-11; squares, triangle and diamonds to subjects 12, 13 & 14 respectively. Horizontal tilts represent tilts around the y-axis, and vertical tilts around x-axis. **B.** Horizontal and vertical decentration of the crystalline lens in 17 eyes of 14 subjects. Solid symbols correspond to right eyes, and open symbols to left eyes, labeled as in Figure 2.11.A. Positive horizontal decentrations represent temporal shifts from the pupil center for the right eye, and nasal for left eyes.

4.5 Intraocular lens tilt and decentration

Figure 2. 12.A shows IOL tilt, and Figure 2. 12.B shows decentration, in eight eyes of five subjects. The sign convention is the same as that for the crystalline lens. IOL horizontal tilt ranged from -0.72 ± 0.08 to 3.6 ± 0.031 deg in right eyes and from -1.51 ± 1.34 to 3.48 ± 0.42 deg in left eyes. Vertical tilt ranged from –1.85 ± 0.52 to 5.97 ± 0.82 deg in right eyes and from 0.75 ± 0.43 to 3.83 ± 0.58 deg in left eyes. IOL decentrations ranged, in the horizontal direction, from -0.31 ± 0.23 to 0.53 ± 0.06 mm in right eyes and 0.23 ± 0.032 to 0.51± 0.04 mm in left eyes. Vertical decentrations ranged from -0.96 ± 0.07 to 0.13± 0.08 mm in right eyes and from -0.96 ± 0.07 to -0.33 ± 0.02 mm in left eyes. Reproducibility of the measurements are 0.6 and 0.55 deg for horizontal and vertical tilt respectively, and 0.06 and 0.05 mm for horizontal and vertical decentration respectively.

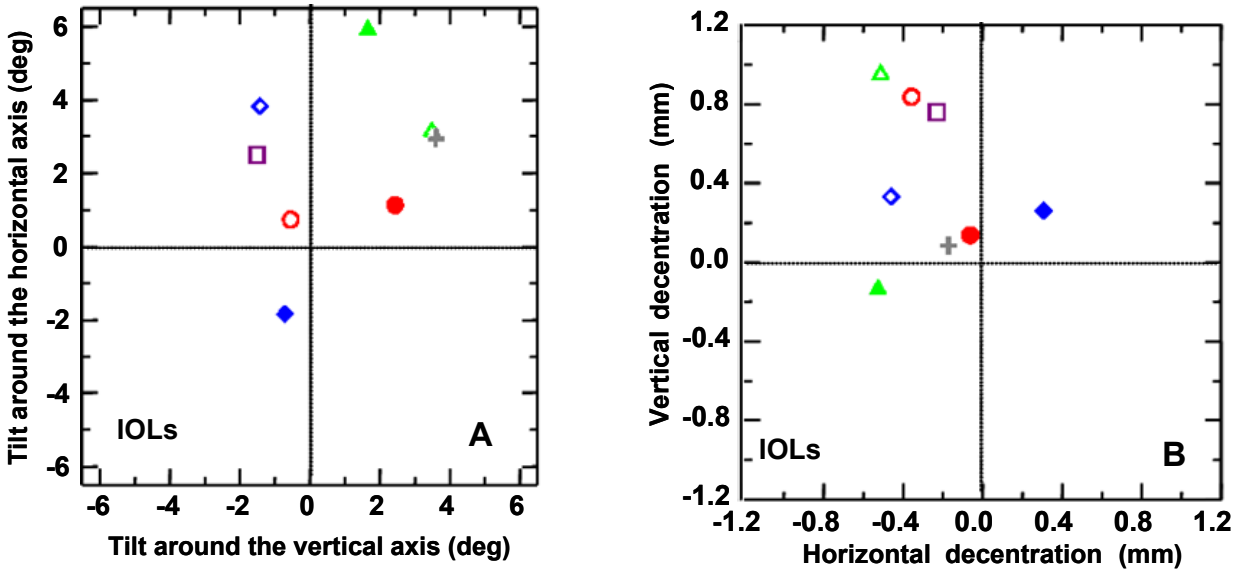

Figure 2.12. A. Tilt around the horizontal and vertical axis of the IOL in eight eyes of five subjects after cataract surgery. Solid symbols correspond to right eyes and spherical IOLs and open symbols correspond to left eyes and aspheric IOLs. Each shape correspond to a different subject. **B.** Horizontal and vertical decentration of the intraocular lens in eight eyes of five subjects after cataract surgery. Solid symbols correspond to right eyes and spherical IOLs and open symbols correspond to left eyes and aspheric IOLs. Each shape corresponds to a different subject. Signs are as in Figure 2.12.A. Error bars are smaller than the symbol size.

5. DISCUSSION

5.1 Comparison with previous studies

A new system is presented, suited for phakometry/positioning measurements of both the crystalline lens and IOLs. The instrument is very compact and well adapted to clinical use. The incorporation of a Badal system and flexible fixation targets can ensure relaxed accommodation. Also, a thorough validation has been performed, using both realistic simulations of the actual intensity distributions of PI, PIII and PIV in the pupillary image, and for the first time, to our knowledge, tilt and decentration data in both the horizontal and vertical directions.

Our analysis shows that the Merit Function provides more accurate data than the Equivalent Mirror method. Our average phakometry results using the merit function method (10.61 ± 1.13mm and -6.15 ± 0.41 mm, for the anterior and posterior lens respectively) can be compared with those reported by other authors. Kirschkamp et al (Kirschkamp et al., 2004) using Barry et al (Barry et al., 2001) Purkinje-image system and the equivalent mirror, reported for the un-acommodated eye (n=9 with age

ranging from 20 to 38 years) radii of 12.3 ± 0.8 mm and -6.01 ± 0.2 mm for the anterior and posterior lens respectively. While the differences are not statistically significant for the posterior lens, our anterior lens radii of curvature are significantly lower. Part of the difference might be due to differences in the age range of both groups. Our phakometry data are comparable with those reported by Smith and Garner (Garner & Smith, 1997) (n=11 with age ranging from 18-38 yr) with average lens radii of curvature of 11.54 ± 1.27 mm and -6.67 ± 0.97 mm for the anterior and posterior lens, respectively. Our data are also consistent with recent reports using different methods. Using distortion-corrected Scheimpflug images in subjects of similar age. Dubbleman and van der Heijde´s (Dubbelman & van der Heijde, 2001) empirical equation yields average anterior and posterior lens radii of 11.37 and -5.87 mm, respectively, for the average age of our subjects. Differences in the posterior lens are not significant. The slight differences in the anterior lens may be due to the fact that Scheimpflug crosssections are fit to conic surfaces, and the apical radius is reported, while the Purkinje system samples more peripheral areas. Also, it should be noted that Scheimpflug images were captured with the subject viewing the fixation stimulus with the contralateral eye. Further analysis of phakometry on a larger sample of young eyes (n=46) will be presented in Chapter 5.

To our knowledge, the only data available in the literature on tilt and decentration of the crystalline lens are those reported by Kisrschkamp (Kirschkamp et al., 2004) and Dunne (Dunne, Davies, Mallen, Kirschkamp & Barry, 2005) for the horizontal direction in two young groups. We report slightly higher values of crystalline lens tilt and larger intersubject variability (1.05 ± 1.12 deg for the horizontal direction and 0.77 ± 1.27 deg for the vertical direction than those reported by Kirschkamp (Kirschkamp et al., 2004) (0.2 ± 0.8 deg, horizontal direction) and Dunne (Dunne et al., 2005) (0.2 ± 1.8 deg, horizontal direction). We also found slightly higher decentrations (0.28 ± 0.12 mm for horizontal decentration and -0.06 ± 0.08 mm for vertical decentration) as opposed to 0.1 ± 0.2 mm reported by Kirschkamp (Kirschkamp et al., 2004) and -0.1 ± 0.1 mm reported by Dunne (Dunne et al., 2005).

Our measurements of IOL tilt and decentrations (0.87 ± 2.16 deg for horizontal tilt, 2.3 ± 2.33 deg for vertical tilt, and, 0.25 ± 0.28 deg for horizontal decentration and -0.41 ± 0.39 mm for vertical decentration) can be compared with those of a few reports using Purkinje imaging or other methods. Those studies typically do not report the direction and sign of tilts and decentrations. Phillips (Phillips et al., 1988) used a Purkinje

imaging system to measure tilt and decentration of posterior chamber IOLs in 13 patients and found average tilts of 7.8 ± 3 deg and decentration of 0.7 ± 0.3 mm. While those estimates are larger than the ones obtained in our study, IOL designs and surgical techniques have evolved tremendously in the last 18 years, and the accuracy in lens positioning has potentially improved. A more recent clinical study measured tilt and decentration after primary and secondary transsclerally sutured posterior chamber IOLs evaluating the Purkinje reflections while the subject was fixating at different locations in a Goldman perimeter (Ismet, 2000). This study reported an average IOL tilt of 5.71 ± 3.41 deg in the first group (14 eyes) and 6.22 ± 3.94 deg in the second group (42 eyes) and average decentrations of 0.67±0.43 mm and 0.59 ±0.43 mm respectively. Those values are larger than those reported in the present study, potentially due to the surgical procedure and implicit assumptions in the methodology using perimetry. More recent studies used commercial Scheimpflug photography to assess tilt and decentration on different types of IOLs, and found estimates consistent with our results. One study (Meng-Chi, Lin-Chung, Chao-Yu & Han-Chin., 1998) reported tilts and decentrations of PMMA and silicone IOLs in 70 eyes, and found average tilts of 2.93 ± 2.68 deg and 3.4 ± 2.02 deg and average decentrations of 0.37 ± 0.19 mm and 0.29 ± 0.26 for the the PMMA and silicone groups respectively). Another study (Kim & Shyn, 2001) evaluated PMMA (n=65), 3-piece silicone (n=47), and 3-piece acrylic (n=25) IOLs, and found average tilts of 2.67 ± 0.84 deg, 2.61± 0.84 deg and 2.69± 0.87 deg, and average decentrations of 0.31 ± 0.15mm, 0.32 ± 0.18 mm, 0.33 ± 0.19 mm, respectively. The average estimates are very similar to those of our study. However the intersubject variability, despite the larger sample of the Scheimpflug studies, seems excessively low. Further analysis of tilt and decentration of IOLs in a larger sample of pseudophakic eyes (n=38) will be presented in Chapter 10.

5.2 Limitations of the technique and implication of the results

A compact optical system has been developed to measure phakometry, and lens tilt and decentration, and demonstrated its use in both normal eyes and eyes with intraocular lenses. Computer simulations have allowed us to test the methodology, the performance of the system, and the validity of the assumptions. The main limitation of the technique comes from the fact of considering spherical surfaces for the lens that produces an overestimation of the lens radii of curvature. Although this limitation may

be important in providing accurate phakometry measurements when larger asphericities are present, we have demonstrated that these differences do not affect tilt and decentration measurements. While this issue could be overcome ensuring that the Purkinje images are formed in the apical zone, in general this is not practically possible since for those angles the Purkinje images typically overlap. Other alternatives are the use of multiple double LEDs with different separations which would allow estimates of radii of curvature as a function of radial distance and therefore estimates of asphericities, and the use of more sophisticated models for equivalent mirror (or better, for the merit function since we have demonstrated that the latter gives more accurate phakometry) incorporating aspheric surfaces. The rest of the factors tested (gradient index of the lens, anterior chamber depth, lens thickness or corneal irregularities) do not seem to have major impact on the measurements.

Although in most of the patients we could successfully measure phakometry, tilt and decentration, there were several eyes with IOLs (not presented here) for which phakometry of the anterior lens was not possible, because the distance between the double PIII exceeded the pupil diameter. Presumably, these IOLs show very flat anterior surfaces. We have estimated that lenses with radii of curvature larger than 20 mm will produce that problem, with the current configuration of LED separation, and for a pupil diameter of 6 mm. Tilt and decentration measurements are possible, provided that nominal anterior radius of curvature is known and that tilt does not exceed 10 deg (for 0 mm decentration and for anterior lens radius of curvature of 10.45mm).

While measurements of phakometry, tilt and decentration of crystalline lenses /IOLs are informative to characterize the normal eye or the outcomes of intraocular surgery, they will become particularly relevant in combination with other optical and geometrical data, to model individual eyes and predict their optical quality, to understand the sources of aberrations, to shed light into the mechanisms of accommodation and to evaluate the potential benefits of different intraocular lens designs.